

Article

A Sliding Mode Controller with Signal Transmission Delay Compensation for the Parallel DC/DC Converter's Network Control System

Juan Yu ¹, Weiqi Zhang ^{2,*}, Wenwen Xiong ¹ and Yanmin Wang ² 

¹ Yatai Construction Science & Technology Consulting Institute Co., Ltd., Beijing 100120, China; yujuan2006708@126.com (J.Y.); yaofeixh@163.com (W.X.)

² School of Electrical Engineering and Automation, Harbin Institute of Technology, Harbin 150001, China; wangyanmin@hit.edu.cn

* Correspondence: 23b906013@stu.hit.edu.cn

Abstract: The network control system (NCS) of the parallel DC/DC converter is always affected by the signal transmission delay, and the ideal output performance is lost. In this paper, a typical parallel buck converter is taken as the research object. Firstly, a sliding mode controller (SMC) in the discrete domain is designed to enhance the robustness of the system. On this basis, the effects of different delays on the stability of the converter's NCS are analyzed, and the actual effects of long/short delays on the converter's NCS are obtained. To further solve the problem of damage to transmitted signals of the NCS by long delay, the SM controller designed in this paper is improved by incorporating a multi-step prediction method. This enhancement enables effective prediction and compensation of the delay signals lost by the NCS, ensuring the output performance of the parallel buck converter. Finally, the superiority of the proposed method is verified by designing simulations and experiments.

Keywords: parallel buck converters; sliding mode control; network control systems; multi-step prediction method



Citation: Yu, J.; Zhang, W.; Xiong, W.; Wang, Y. A Sliding Mode Controller with Signal Transmission Delay Compensation for the Parallel DC/DC Converter's Network Control System. *Electronics* **2024**, *13*, 121. <https://doi.org/10.3390/electronics13010121>

Academic Editors: Mahmut Reyhanoglu, Mohammad Jafari and Erkan Kayacan

Received: 9 October 2023

Revised: 5 December 2023

Accepted: 15 December 2023

Published: 28 December 2023



Copyright: © 2023 by the authors. Licensee MDPI, Basel, Switzerland. This article is an open access article distributed under the terms and conditions of the Creative Commons Attribution (CC BY) license (<https://creativecommons.org/licenses/by/4.0/>).

1. Introduction

The parallel DC/DC converter finds extensive application across various domains, including electric vehicles, photovoltaic systems, telecommunication base stations, and other electric energy conversion fields [1,2]. Its remarkable attributes include the mitigation of physical stress on the converter during energy flow by employing voltage equalization and parallel techniques [3,4]. Consequently, these features contribute to the enhancement of the converter's output power [5,6].

In engineering applications, network control systems (NCSs) are employed to manage parallel DC/DC converters because of their ease of deployment and operation [7,8]. Since the control signals for parallel DC/DC converters as well as the status signals from sensors and actuators are transmitted via network channels, the network transmission is often assumed to be ideal during the system design phase [9,10]. However, practical experience reveals that, owing to limitations in network bandwidth and signal processing speed, network controllers exhibit signal transmission delays, resulting in packet loss [10,11]. This phenomenon significantly impairs the stability of the control system's output [12,13]. Furthermore, the network signal transmission delay and packet loss rate are influenced by various factors that change over time, rendering them highly uncertain [14,15]. Given the random occurrence of network transmission delays and packet losses, selecting and adjusting the signal sampling period for parallel DC/DC converters is a formidable challenge. This not only impacts the quality of the converter's output power but also hampers the overall control performance enhancement of the NCS [16,17].

When comparing the delay in network transmission with the system sampling period, the delay can be categorized into two types: short delay and long delay. Short delay refers to cases where the signal transmission delay is less than or equal to a single sampling period, while long delay occurs when the delay exceeds the sampling period [18,19]. Addressing the impact of these different delays on NCS has emerged as a prominent research area. Initially, Pang et al. assumed that the signal transmission delay between the sensor, controller, and actuator made up a short delay. Accordingly, they developed a controller that considered the impact of this delay. However, this method's reliance on the assumption of only short delays overlooked the possibility of encountering long delays, thereby imposing limitations on its effectiveness [20]. Yan et al. designed an event-triggered H_∞ controller for NCSs with network channel delay. The network channel delay is modeled as a distributed delay with a probability density function as its kernel, and the closed-loop event-triggered control system is established as a distributed delay system. However, the method proposed in the literature is based on the continuous domain without exploiting the potential influence of discretization on the stability of the event-triggered H_∞ controller. Hence, the implementation and application performance of the designed method is reduced [21]. Kim et al. proposed a new method to obtain a maximum allowable delay bound for the scheduling of NCSs. The method is planned in terms of linear matrix inequalities and can provide a much less conservative delay bound than the existing methods, and a network scheduling method is presented based on the delay obtained through the proposed method. However, the method of obtaining the transmission delay of NCSs is not clearly provided in the literature, and only the estimated delay length is used to assign network nodes to the transmission signal of the system, which reduces the reliability of the system [22]. Heemels et al. presented a general framework that incorporates communication constraints, varying transmission intervals and varying delays, and an explicit construction of a continuum of Lyapunov functions is provided based on a newly developed NCS model including all these network phenomena, then the maximally allowable transmission interval and the maximally allowable delay to guarantee stability of the NCS in the presence of communication constraints. However, the literature has not put forward an exact and effective solution for different transmission intervals and delays [23]. Bibhu et al. presented the development of a novel synchrophasor measurement-based wide-area centralized damping controller to improve the stability of a power system in the presence of time-varying delay and packet dropout in the communication network. This method depends on the measurement of the transmission delay itself, which requires high precision of the control system [24]. In this literature [25], a networked predictive control strategy is proposed for discrete networked systems to deal with the random delay. However, this method treats the network transmission delay as a fixed delay and cannot be applied to complex network delays. Based on the analysis provided, most studies predominantly focus on the continuous time domain, neglecting the discrete state of NCSs and the nuanced performance analysis concerning various types of delays affecting the system. And the problem of measuring the transmission delay of the system has become a difficult problem restricting the design of the controller, the challenge of effectively compensating random delays in control signals of NCSs requires further improvement. This paper systematically considers the practicability of continuous domain control design and discrete domain controller transformation, analyze the impact of different types of delay on the system NCS, and use the signal retention characteristics of the sensor to avoid the measurement of transmission delay.

A large amount of literature shows that the application of sliding mode control (SMC) in parallel DC/DC converters combines robustness, fast response, and enhanced current-sharing capabilities. These advantages make the SMC strategy an attractive choice for enhancing the performance and reliability of parallel DC/DC converter systems [26,27]. The literature [28] proposes a novel nonlinear control method for the input-parallel output-series modular dual active bridge DC/DC converter, which regulates the DC-bus voltage and individual module voltages together. A uniform quantization design method for the

parallel text DC-DC converter’s NCS is proposed in [29] in combination with the SMC strategy to solve the problem that the performance of the system is poor. The literature [30] shows the analysis and design of a parallel-connected converter system using sliding mode control techniques. And a new general SMC is proposed for the DC-DC converter that can regulate the output voltage in the literature [31]. The literature [32] also presents a control design procedure for DC-DC power converters, which develops SMC algorithms for several types of DC-DC converters with different control objectives, and complete and incomplete information about system states.

In this paper, a discrete domain SM current-sharing controller based on linear sliding mode control (LSMC) strategy is designed for the parallel DC/DC converter’s NCS, with the buck type being used as an example. The study focuses on analyzing the impact of uncertain and random transmission delays on performing the parallel buck converter’s NCS, particularly in the presence of system disturbances. To address this, a multi-step prediction method is employed for compensating the delay signal in the NCS. The article makes the following specific contributions:

- Considering a parallel buck converter’s NCS with a random time delay, a master-slave current-sharing controller is designed based on the LSMC in the continuous domain. Then the zero-order holder (ZOH) is used to realize the discretization of the designed system, and the stability conditions of the discrete system are further determined through the Lyapunov equation;
- Based on the length characteristics of different transmission delays, the effects of uncertainty and randomness on performing parallel buck converter’s NCS with system disturbance are analyzed, which lays a foundation for the design of delay compensation strategy;
- In order to solve the problem of the influence of random delay on the system stability, the LSM controller is improved based on the multi-step prediction method, and the system parameter conditions are provided based on analyzing the stability of the designed control system;
- Designed simulations and experiments prove the effectiveness of the proposed method.

2. Design of SMC for the Parallel DC/DC Converter

This paper takes a typical n -phase parallel buck converter system as an example of designing its NCS. The overall structure of the system is shown in Figure 1 below.

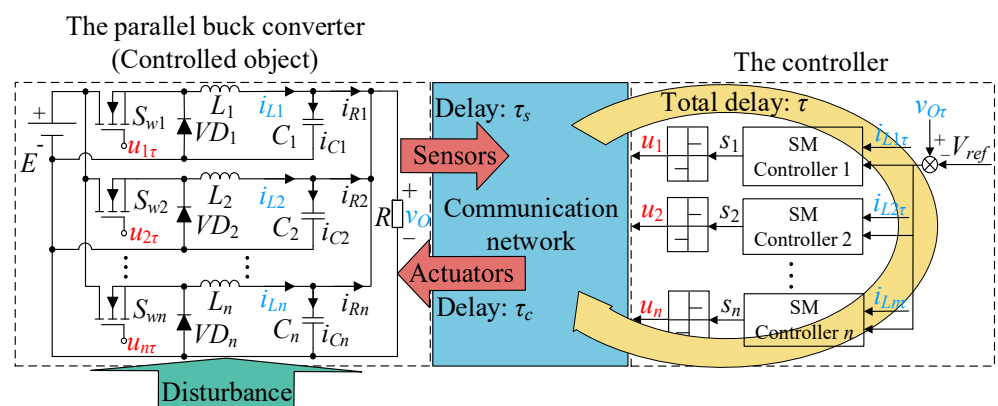


Figure 1. An NCS with transmission delays of the n -phase parallel buck converter.

In Figure 1, E is the DC input voltage source; v_O is the output voltage of the parallel buck converter; R is the load resistance; L_i and C_i represent the filter inductance and capacitance of phase i ($i = 1, 2, \dots, n$), respectively; i_{L_i} and i_{C_i} represent the current flowing through L_i and C_i , respectively; i_{R_i} indicates the current output of each phase to load R , and satisfying $i_{R_i} = i_{L_i} - i_{C_i}$; VD_i is phase i continuous current diode; S_{wi} represents the phase i switching power tube, often used by N-MOSFET or IGBT, whose “on” and “off” state are

controlled by the “1” and “0” pulses of the signal u_i ; V_{ref} represents the output reference voltage of the converter; and s_i is the system state variable output by the SM controller.

In order to be closer to the real NCS, the time delay of signal transmission between the feedforward channel and the feedback channel is considered in Figure 1, and it is assumed that the delay from the sensor to the controller is τ_s , the delay from the controller to the actuator is τ_c . In fact, if the feedback control system can maintain static properties, these two delays can be lumped together as $\tau = \tau_s + \tau_c$, and the τ is the total delay in the NCS [31]. For the convenience of description, the subscript “ τ ” is used to represent signals with transmission delays, such as $i_{Li\tau}$, $v_{O\tau}$, and $u_{i\tau}$. It should be noted here that the delay τ does not change the characteristics of the signal itself, such as $u_{i\tau}$ and u_i are all output “1” or “0” control signals.

2.1. Modeling of the Parallel Buck Converter System

In order to facilitate the analysis of the energy flow process of the converter, the switching loss of the converter is ignored here, and it is assumed that the parallel buck converter works in continuous current mode (CCM), and each phase control signal u_τ is generated by the same pulse width modulation (PWM). Thus, the output current of each phase of the system can meet $i_{Ri} = v_O/(nR)$. By analyzing the working process of the converter when the power tube S_{wi} is switched on and off, and combining Kirchhoff’s circuit law and the characteristics of L_i and C_i components, the following converter model can be obtained:

$$S_{wi} \text{ on } \begin{cases} \frac{di_{Li}}{dt} = \frac{1}{L_i}(E - v_O) \\ \frac{dv_O}{dt} = \frac{1}{C_i}i_{Ci} = \frac{1}{C_i}(i_{Li} - i_{Ri}) \end{cases}, S_{wi} \text{ off } \begin{cases} \frac{di_{Li}}{dt} = -\frac{1}{L_i}v_O \\ \frac{dv_O}{dt} = \frac{1}{C_i}(i_{Li} - i_{Ri}) \end{cases} \quad (1)$$

Using the characteristic of control signal $u_{i\tau}$ output “0” or “1”, and substituting $i_{Ri} = v_O/(nR)$ into (1), then the system model can be represented uniformly as:

$$\begin{bmatrix} \frac{di_{Li}}{dt} \\ \frac{dv_O}{dt} \end{bmatrix} = \begin{bmatrix} 0 & -\frac{1}{L_i} \\ \frac{1}{C_i} & -\frac{1}{nRC_i} \end{bmatrix} \begin{bmatrix} i_{Li} \\ v_O \end{bmatrix} + \begin{bmatrix} \frac{E}{L_i} \\ 0 \end{bmatrix} u_{i\tau} \quad (2)$$

2.2. Design of the SM Controller

Due to the simple structure of LSM, the impulse switching control of $u_{i\tau}$ signal can be satisfied on the basis of ensuring the robustness of the system [29]. Therefore, this paper adopts the LSM to design the parallel DC/DC converter control system in the continuous domain. For the circuit topology is shown in Figure 1, the phase i is taken as the object, and the output voltage deviation and its derivative of the phase i are respectively defined as state variables $x_{1i\tau}$ and $x_{2i\tau}$ as:

$$\begin{cases} x_{1i\tau} = v_{O\tau} - V_{ref} \\ x_{2i\tau} = \dot{x}_{1i\tau} = \dot{v}_{O\tau} \end{cases} \quad (3)$$

where V_{ref} is the reference value of the output voltage $v_{O\tau}$ of the converter; $x_{1i\tau}$ and $x_{2i\tau}$ are bounded variables and satisfy $|x_{1i\tau}| \leq \psi_{x1i\tau}$ and $|x_{2i\tau}| \leq \psi_{x2i\tau}$, $\psi_{x1i\tau} > 0$ and $\psi_{x2i\tau} > 0$ are boundary constants. By further substituting (2) into (3), the state space model of the buck system can be obtained as:

$$\dot{x}_{i\tau}(t) = A_i x_{i\tau}(t) + b_i u_{i\tau}(t) + f_i + \zeta_i(t) \quad (4)$$

where the state vector $x_{i\tau}(t) = [x_{1i\tau}(t), x_{2i\tau}(t)]^T$, and there is $\|x_{i\tau}(t)\| \leq \psi_{x_{i\tau}}$, $\psi_{x_{i\tau}} = [\psi_{x1i\tau}, \psi_{x2i\tau}]^T$ is the boundary constant vector; $\zeta_i(t)$ is the matching disturbance of the system, which satisfying $\zeta_i(t) = b_i \delta_i(t)$, where δ_i is the actual bounded disturbance of the external

input, which satisfying $|\delta_i(t)| \leq \beta_i$, and β_i is the upper bound constant. The coefficient matrix A_i , b_i , and f_i can be expressed as:

$$A_i = \begin{bmatrix} 0 & 1 \\ -\frac{1}{L_i C_i} & -\frac{1}{nRC_i} \end{bmatrix}, b_i = \begin{bmatrix} 0 \\ \frac{E}{L_i C_i} \end{bmatrix}, f_i = \begin{bmatrix} 0 \\ -\frac{V_{ref}}{L_i C_i} \end{bmatrix} \quad (5)$$

The design of LSMC generally includes LSM surface and control law. And the LSM surface of the system can be designed by the state variables in (4) as:

$$s_i(t) = \lambda_i x_{1i\tau}(t) + x_{2i\tau}(t) + k_i \int_0^t x_{1i\tau}(t) dt \quad (6)$$

where $s_i(t)$ is the sliding variable of the phase i controller; λ_i and k_i are the coefficients of the SM surface, and satisfying $\lambda_i > 0$ and $k_i > 0$.

Remark 1. It should be noted that λ_i can be used to adjust the convergence rate of the $s_i(t)$ of the system, but the chattering of the system state will also be aggravated with the increase in λ_i . Hence the integral term is introduced in (6) to help adjust the steady-state error of the system output and further enhance the robustness of SMC. And it is necessary to analyze the motion characteristics of the designed sliding surface in (6):

When the system state reaches the preset SM surface $s_i(t) = 0$, it can be obtained that:

$$\ddot{x}_{1i\tau}(t) + \lambda_i \dot{x}_{1i\tau}(t) + k_i x_{1i\tau}(t) = 0 \quad (6a)$$

Here defining $x_{1i\tau}(0)$ and $x_{2i\tau}(0) = \dot{x}_{1i\tau}(0)$ as the initial values of $x_{1i\tau}(t)$ and $x_{2i\tau}(t)$. By introducing the Laplace transform, can we get the unique solution to (6a) as:

$$x_{1i\tau}(t) = \frac{x_{1i\tau}(0) \left(2 - \lambda_i + \sqrt{\lambda_i^2 - 4k_i} \right) + \dot{x}_{1i\tau}(0) e^{-\lambda_i + \frac{\sqrt{\lambda_i^2 - 4k_i}}{2} t}}{2\sqrt{\lambda_i^2 - 4k_i}} + \frac{x_{1i\tau}(0) \left(2 - \lambda_i - \sqrt{\lambda_i^2 - 4k_i} \right) + \dot{x}_{1i\tau}(0) e^{-\lambda_i - \frac{\sqrt{\lambda_i^2 - 4k_i}}{2} t}}{-2\sqrt{\lambda_i^2 - 4k_i}} \quad (6b)$$

It can be obviously seen from (6b) that the coefficient k_i can be used to adjust the convergence rate of the exponential terms in each term, which not only avoids the chattering problem caused by the use of larger λ_i , but also clearly provides the limit range $\lambda_i^2 > 4k_i$ of λ_i , i.e., the selection of k_i should also be smaller to improve the output accuracy of the system.

As for the control law $u_{si\tau}(t)$ of the LSMC in the phase i , which is usually composed of the equivalent control law $u_{eqi\tau}(t)$ and the switching control law $u_{Ni\tau}(t)$. In the process of system convergence, the system state rapidly reaches the preset SM surface $s_i(t) = 0$ under the action of $u_{eqi\tau}(t)$, and then moves along $s_i(t) = 0$ under the action of $u_{Ni\tau}(t)$ to the convergence point. Combining the above state motion characteristics of the SMC system, $u_{eqi\tau}(t)$ can be obtained by finding the zero crossing of the first derivative of $s_i(t)$ in (6). Therefore, the first derivative of $s_i(t)$ and the system state variable in (3) can be substituted into it as:

$$\dot{s}_i(t) = -\frac{1}{L_i C_i} x_{1i\tau}(t) + \left(\lambda_i - \frac{1}{nRC_i} \right) x_{2i\tau}(t) + \frac{E}{L_i C_i} u_{si\tau}(t) - \frac{V_{ref}}{L_i C_i} + \frac{E}{L_i C_i} \delta_i(t) \quad (7)$$

In (7), if $\dot{s}_i(t)|_{u_{eqi\tau}} = 0$, the expression of $u_{eqi\tau}(t)$ can be expressed as:

$$u_{eqi\tau}(t) = \frac{1}{E} x_{1i\tau}(t) - \frac{L_i C_i}{E} \left(\lambda_i - \frac{1}{nRC_i} \right) x_{2i\tau}(t) + \frac{V_{ref}}{E} - \delta_i(t) \quad (8)$$

Considering the switching characteristics of the parallel buck converter corresponding to (1), $u_{Ni\tau}(t)$ can be further designed as:

$$u_{Ni\tau}(t) = -\eta_i \text{sgn}[s_i(t)] \quad (9)$$

where η_i is the switching control gain and satisfying $\eta_i > 0$. By combining (8) and (9), the control law $u_{si\tau}(t)$ of LSM can be obtained as:

$$u_{si\tau}(t) = u_{eqi\tau}(t) + u_{Ni\tau}(t) = k_{PWM}u_{i\tau}(t) \tag{10}$$

where k_{PWM} represents the required gain after the continuous control signal $u_{si\tau}(t)$ is converted into the switching signal $u_{i\tau}(t)$ by PWM. According to the literature [33], $u_{si\tau}(t)$ is essentially the switching duty cycle of the converter, so the LSMC designed in this paper is essential to adjust the output voltage of the system by controlling the switching duty cycle of the parallel buck converter.

2.3. Discretization and Stability Analysis of the System

In order to further expand the application of the designed SMC system in digital circuits and facilitate the analysis of the transmission delay process of the NCS, the SMC of the parallel buck converter designed in (4), (6), and (10) will be discretized. Here the ZOH is used to discretize the system, and system states in (4) can be transformed into:

$$x_{i\tau}[(k + 1)h] = \Phi_i x_{i\tau}(kh) + \Gamma_i u_{si\tau}(kh) + \Lambda_i + \Gamma_i \delta_i(kh) \tag{11}$$

where $x_{i\tau}(kh) = [x_{1i\tau}(kh), x_{2i\tau}(kh)]^T$ represents the state of the discrete system, and relationship of $\|x_{i\tau}(kh)\| \leq \psi_{xi\tau}$ is held; $u_{si\tau}(kh)$ stands for the discrete control law; h is the signal sampling period, and satisfying $0 < h \ll 1$; the expressions of the discrete coefficient matrix Φ_i , Γ_i and Λ_i can be expressed as:

$$\begin{cases} \Phi_i = e^{A_i h} = I + \int_0^h e^{A_i t} dt A_i = I + A_i h + A_i^2 \frac{h^2}{2!} + O(h^3) \\ \Gamma_i = \int_0^h e^{A_i t} dt b_i = b_i h + A_i b_i \frac{h^2}{2!} + O(h^3) \\ \Lambda_i = \int_0^h e^{A_i t} dt f_i = f_i h + A_i f_i \frac{h^2}{2!} + O(h^3) \end{cases} \tag{12}$$

where $O(h^3)$ is the third-order infinitesimal of h . Since the h always remains unchanged during the operation of the discrete system, it can be regarded as a constant value in theory, and (11) can be further simplified as:

$$x_{i\tau}(k + 1) = \Phi_i x_{i\tau}(k) + \Gamma_i u_{si\tau}(k) + \Lambda_i + \Gamma_i \delta_i(k) \tag{13}$$

Similarly, the LSMC designed in (6), (8) and (9) can be discretized by ZOH, and discrete SM surface $s_i(k)$, discrete equivalent control law $u_{eqi\tau}(k)$ and discrete switching control law $u_{Ni\tau}(k)$ can be obtained respectively as:

$$s_i(k) = \lambda_i x_{1i\tau}(k) + x_{2i\tau}(k) + k_i \sum_{k=0}^t x_{1i\tau}(k) = c_i x_{i\tau}(k) \tag{14}$$

$$u_{eqi\tau}(k) = (c_i \Gamma_i)^{-1} [-c_i (\Phi_i - I) x_{i\tau}(k) - c_i \Lambda_i - c_i \Gamma_i \delta_i(k)] \tag{15}$$

$$u_{Ni\tau}(k) = -\eta_i \text{sgn}[s_i(k)] \tag{16}$$

where the parameter matrix $c_i = [\lambda_i + k_i S_{x_i}, 1]$, S_{x_i} is the sum operator of discrete variables. The discrete SM control law $u_{si\tau}(k) = u_{eqi\tau}(k) + u_{Ni\tau}(k)$ can be obtained from (15) and (16).

Remark 2. The sum operator S_x represents summing the discrete variables of the system throughout sampling time, which is introduced in (14) for simplifying the formula expression of the discrete system and satisfies:

$$S_x \mathbf{x}_{i\tau}(k) = \sum_{k=0}^t \mathbf{x}_{i\tau}(k) = \sum_{k=0}^t (x_{1i\tau}(k) + x_{2i\tau}(k)) = \sum_{k=0}^t x_{1i\tau}(k) + \sum_{k=0}^t x_{2i\tau}(k) \quad (16a)$$

It is worth noting that S_x belongs to the bounded operator when applied to discrete variables, and the following relationship can be obtained:

$$\sum_{k=0}^t |S_x \mathbf{x}_{i\tau}(k)|^2 = \sum_{k=0}^t \left| \sum_{k=0}^t \mathbf{x}_{i\tau}(k) \right|^2 \leq \sum_{k=0}^t \left(\sum_{k=0}^t |\mathbf{x}_{i\tau}(k)|^2 \right) \leq \sum_{k=0}^t \left(\sum_{k=0}^t |\boldsymbol{\psi}_{xi\tau}|^2 \right) \quad (16b)$$

It can be further deduced from (16b) that:

$$\|S_x \mathbf{x}_{i\tau}(k)\| \leq \|\boldsymbol{\psi}_{xi\tau}\| \xrightarrow{\|\mathbf{x}_{i\tau}(k)\| \leq \|\boldsymbol{\psi}_{xi\tau}\|} \|S_x\| \leq 1 \quad (16c)$$

Since the summation form $S_x \mathbf{x}_{i\tau}$ corresponds to the integral operation $\int \mathbf{x}_{i\tau} dt$ in the continuous field, it needs to be emphasized here that $S_x \mathbf{x}_{i\tau}$ is satisfied when the forward difference or the backward difference is checked and divided (the backward difference was divided into examples):

$$\frac{S_x \mathbf{x}_{i\tau}(k) - S_x \mathbf{x}_{i\tau}(k-1)}{h} = \frac{\sum_{k=0}^t \mathbf{x}_{i\tau}(k) - \sum_{k=0}^t \mathbf{x}_{i\tau}(k-1)}{h} = \mathbf{x}_{i\tau}(k) \quad (16d)$$

It can be seen from (16d) that introducing the sum operator does not change the properties of each variable and is only used to represent the operation process.

The stability of the discretized system will be analyzed below. First, the Lyapunov equation V_i can be designed as:

$$V_i(k) = s_i^2(k) \quad (17)$$

In order to ensure that the system state in the discrete domain can converge under the action of the LSMC, (17) must meet the following conditions [29]:

$$\Delta V_i(k) = s_i^2(k+1) - s_i^2(k) < 0 \quad (18)$$

By substituting (13) into (14), the $s_i(k+1)$ can be obtained as:

$$\begin{aligned} s_i(k+1) &= \mathbf{c}_i \boldsymbol{\Phi}_i \mathbf{x}_{i\tau}(k) + \mathbf{c}_i \boldsymbol{\Gamma}_i u_{si\tau}(k) + \mathbf{c}_i \boldsymbol{\Lambda}_i + \mathbf{c}_i \boldsymbol{\Gamma}_i \delta_i(k) \\ &= s_i(k) + \mathbf{c}_i (\boldsymbol{\Phi}_i - \mathbf{I}_i) \mathbf{x}_{i\tau}(k) + \mathbf{c}_i \boldsymbol{\Gamma}_i u_{si\tau}(k) + \mathbf{c}_i \boldsymbol{\Lambda}_i + \mathbf{c}_i \boldsymbol{\Gamma}_i \delta_i(k) \end{aligned} \quad (19)$$

Theorem 1. For the discrete LSMC system designed in (14)–(16), if the sampling period h meets $h < 2nRC_i$, the state of the discrete system can converge along the preset SM surface in finite steps.

Proof of Theorem 1. By substituting $u_{si\tau}(k)$ and (19) into (18), $\Delta V_i(k)$ can be rewritten as:

$$\Delta V_i(k) = \{s_i(k) - \mathbf{c}_i \boldsymbol{\Gamma}_i \eta_i \operatorname{sgn}[s_i(k)]\}^2 - s_i^2(k) = -2\mathbf{c}_i \boldsymbol{\Gamma}_i \eta_i |s_i(k)| + (\mathbf{c}_i \boldsymbol{\Gamma}_i \eta_i)^2 \quad (20)$$

In (20), the term $O(h^3)$ of $\boldsymbol{\Gamma}_i$ can be ignored. Taking into account the opposite effect of $(\mathbf{c}_i \boldsymbol{\Gamma}_i \eta_i)^2$ on the negative of $\Delta V_i(k)$, it is possible to subtract it from (20) and subsequently transform (20) by substituting (12) into it in the following manner:

$$\Delta V_i(k) > -2\mathbf{c}_i \boldsymbol{\Gamma}_i \eta_i |s_i(k)| \geq -2 \left[\frac{Eh}{L_i C_i} + (\lambda_i + k_i S_{xi}) \frac{Eh^2}{2L_i C_i} - \frac{Eh^2}{2nRL_i C_i^2} \right] \eta_i |s_i(k)| \quad (21)$$

Due to the switching control gain $\eta_i > 0$ in (21), when the system state does not reach the SM surface, that is, when $s_i(k) \neq 0$, in order to ensure the establishment of Lyapunov stability theorem $\Delta V_i(k) < 0$, the following relationship must be satisfied:

$$\frac{Eh}{L_i C_i} + \frac{\lambda_i E h^2}{2L_i C_i} + \frac{k E h^2}{2L_i C_i} - \frac{E h^2}{2n R L_i C_i^2} > \frac{Eh}{L_i C_i} - \frac{E h^2}{2n R L_i C_i^2} > 0 \rightarrow h < 2n R C_i \quad (22)$$

By combining the parameter attribute of E, L_i, C_i, λ_i in (22), it is easy to get that the limited range $h < 2n R C_i$ of h . Thus $s_i^2(k+1) < s_i^2(k)$ in (18), i.e., $\|s_i(k+1)\| < \|s_i(k)\|$, hence $\|s_i(k)\|$ decreases monotonously and after a finite number of steps, the system state will enter the admissible domain where $\|s_i(k)\| \rightarrow 0$, and the subsequent part of the state trajectory will be in $s_i(k) = 0$ under $u_{eqi\tau}(k)$ and discrete-time sliding mode will take place.

It is clear from (22) that the stability of the discrete system is influenced by h . The circuit parameters of the parallel buck converter dictate the maximum permissible value for h . In real-world applications, setting h excessively large is not advisable, as it compromises the desirable output performance of the LSMC system. \square

3. Analysis of the Influence of Signal Transmission Delay on the System

The signal transmission delay in a discrete NCS can be categorized into two types: short delay and long delay. Short delay occurs when the signal transmission delay is less than or equal to one sampling period, while long delay occurs when the delay exceeds one sampling period. In the forthcoming simulations designed in Matlab/Simulink, the paper will conduct a detailed analysis of how both short and long transmission delays impact the performance of the discrete NCS system designed in (14)–(16). The focus of this study is on the three-phase parallel buck converter, and the circuit parameters are presented in Table 1 below.

Table 1. System parameters of the parallel buck converter.

Parameter	Value
Load resistance R	10 Ω
Filter inductance L_i	1 mH
Filter capacitance C_i	1000 μF
Reference voltage V_{ref}	10 V
Input DC voltage E	20 V

3.1. Analysis of the Influence of the Short Delay on the NCS

Considering the stability condition of the discrete system in (21), the sampling period $h = 0.1$ ms is selected here, and the transmission delay τ of the parallel buck converter NCS is within two random delay intervals $[0, 0.05$ ms] and $[0, 0.1$ ms], and the τ determined instantaneously in the current step is randomly split into τ_s and τ_c to ensure the reliability of the simulation system. In order to further highlight the effect of different random short delays on the system output performance, the case of no delay is added as a control group. The simulation results are shown in Figure 2 and Table 2.

Table 2. Effect of different delays on output performances of the NCS.

Delay Type	τ (ms)	$\Delta v_{O\tau}$ (V)	$\Delta i_{L_i\tau}$ (A)	System Current Mode
no delay	-	0.07	0.21	CCM
short delay	0.05	0.09	0.38	CCM
	0.10	0.12	0.57	CCM
long delay	0.20	0.22	1.02	CCM
	0.40	0.31	1.29	DCM
	0.60	0.35	1.61	DCM

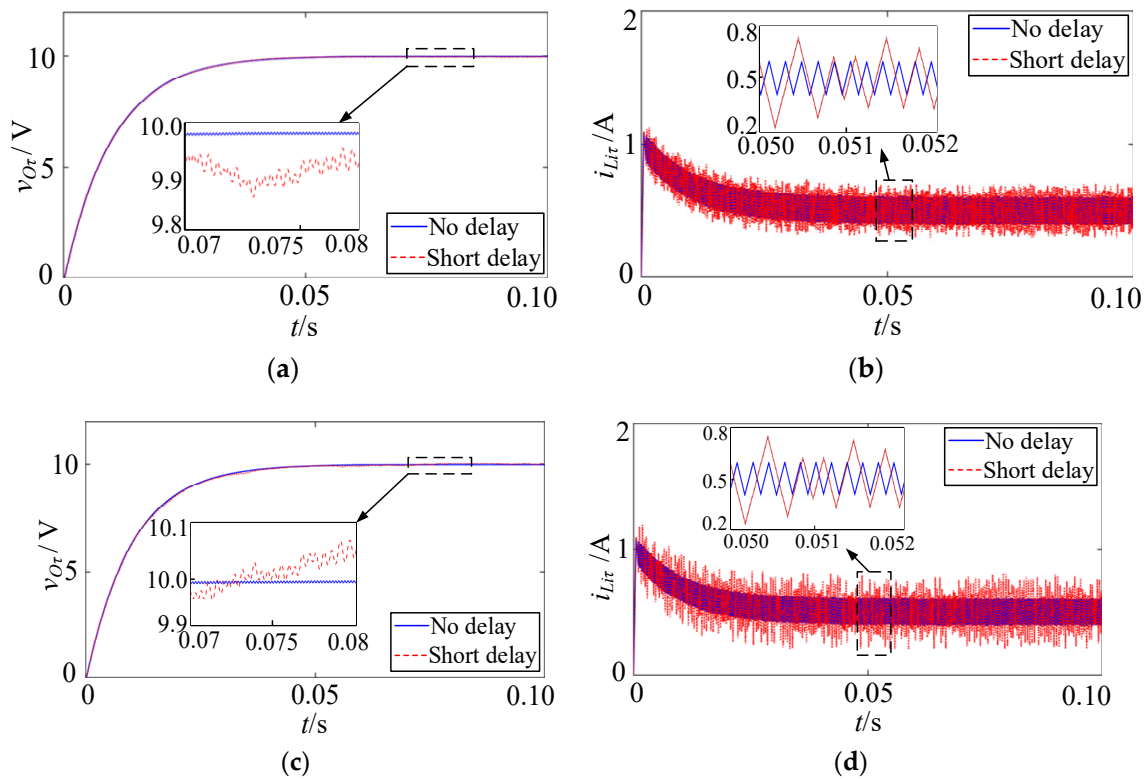


Figure 2. System output performances in random short delay interval: (a) $v_{O\tau}$ in 0.05 ms delay; (b) $i_{Li\tau}$ in 0.05 ms delay; (c) $v_{O\tau}$ in 0.1 ms delay; (d) $i_{Li\tau}$ in 0.1 ms delay.

From the output voltage $v_{O\tau}$ shown in Figure 2a,c, it is observed that when the transmission delay τ randomly falls within the range of 0–0.05 ms and 0–0.1 ms, the $v_{O\tau}$ remains essentially the same in both cases. This observation is further supported by the steady-state errors $\Delta v_{O\tau}$, as observed in Table 2, which amount to 0.09 V and 0.12 V, respectively. These errors closely approach the output performance in the absence of any delay. It can be concluded that short delays have minimal impact on the system output $v_{O\tau}$, thus rendering its influence negligible in practical engineering applications.

Figure 2b,d display the system inductance current $i_{Li\tau}$ under different short delays. According to the data presented in Table 2, the maximum ripple amplitude $\Delta i_{Li\tau}$ at random time delays within the interval [0, 0.05 ms] and [0, 0.1 ms] amounts to 0.38 A and 0.57 A, respectively, both of which exceed the value of 0.21 A observed in the absence of time delay. This amplitude of $\Delta i_{Li\tau}$ gradually increases with increasing delay duration. It is important to note that the system continues to operate under CCM in both cases. This observation signifies that the system can maintain a continuous current output even in the presence of short delays, with the output voltage being essentially unaffected.

3.2. Analysis of the Influence of Long Delay on the NCS

With $h = 0.1$ ms unchanged, three kinds of random delay τ of different lengths [0, 0.2 ms], [0, 0.4 ms], and [0, 0.6 ms] were added to the system, respectively, τ_s and τ_c are also randomly obtained from τ in the current step, and a delay-free group is also added for control. The simulation results are shown in Figure 3 and Table 2 below.

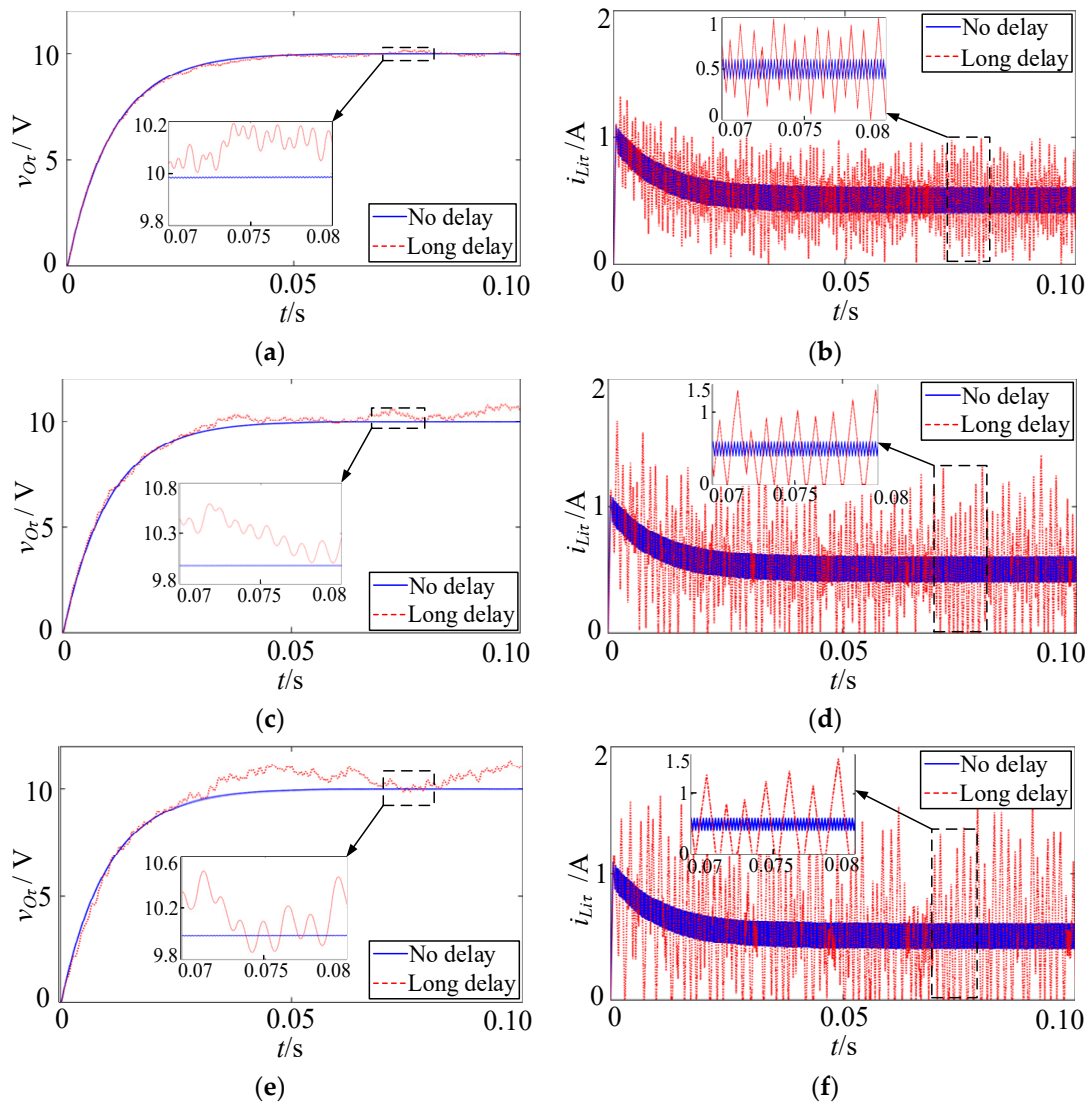


Figure 3. System output performances in random long delay interval: (a) $v_{O\tau}$ in 0.2 ms delay; (b) $i_{Li\tau}$ in 0.2 ms delay; (c) $v_{O\tau}$ in 0.4 ms delay; (d) $i_{Li\tau}$ in 0.4 ms delay; (e) $v_{O\tau}$ in 0.6 ms delay; (f) $i_{Li\tau}$ in 0.6 ms delay.

The impact of random long delays on the stability of the NCS is evident in the findings presented in Figure 3. In the scenarios depicted in Figure 3a,b, when the random long delay falls within the range of [0, 0.2 ms], the output current error $\Delta i_{Li\tau}$ of phase i reaches 1.02 A. Despite this, the system operates within CCM, maintaining a steady state error $\Delta v_{O\tau}$ of 0.22 V. During this period, the system exhibits fundamental stability.

Contrastingly, as illustrated in Figure 3c,e, when the random long delay extends to [0, 0.4 ms] or [0, 0.6 ms], the system’s output voltage $v_{O\tau}$ experiences significant fluctuations. The corresponding $\Delta v_{O\tau}$ values reach 0.31 V and 0.35 V, respectively. Examination of the $i_{Li\tau}$ diagrams in Figure 3d,f reveals that, in both delay cases, $\Delta i_{Li\tau}$ surpasses 1.2 A, indicating a transition to discontinuous current mode DCM and consequent system instability.

These observations emphasize the substantial impact of prolonged delays on the NCS. Notably, as the delay length increases relative to the sampling period h , the system’s stability deteriorates. In summary, the findings underscore the critical role of delay management in preserving the stability of the NCS.

4. Transmission Delay Compensation Strategy Based on Multi-Step Prediction Method

Based on the analysis above, it can be concluded that while the impact of short delays can be negligible, long delays significantly deteriorate the steady-state performance of the NCS. To mitigate this issue, this study proposes a multi-step prediction method with SMC to analyze the current system state and predict the system state backwards in multiple sampling periods. By doing so, the lost control signal because of transmission delay can be compensated, ensuring the desired output performance of the system.

4.1. Design of the Sliding Mode Controller Based on Multi-Step Prediction Method

For bounded delay τ ($\tau > h$), which can be expressed as a multiple of sampling period h relations, i.e., $\tau = (d' + l)h$, where the $d' \in [1, M - 1] \in \mathbf{N}^+$, $l \in [0, 1)$ and M is the upper limit positive integers of $(d' + l)$. Due to the random variation in l , τ is not always an integer multiple of h . To simplify the analysis and design, this study compensates l to 1, resulting in $\tau = dh$, where $d \in [2, M] \in \mathbf{N}^+$. It should be noted that this compensation for l does not significantly alter the original influence of long delay τ on the system, as shown in Figure 3. Therefore, the discrete model of the system in (13) can be re-expressed as:

$$x_{i\tau}(k + 1) = \Phi_i x_{i\tau}(k) + \Gamma_i u_{si\tau}(k - d) - \Gamma_i \frac{V_{ref}}{E} + \Gamma_i \delta_i(k) \tag{23}$$

The delay compensation of the system will be realized based on the multi-step prediction method, and its specific working principle is shown in Figure 4 below:

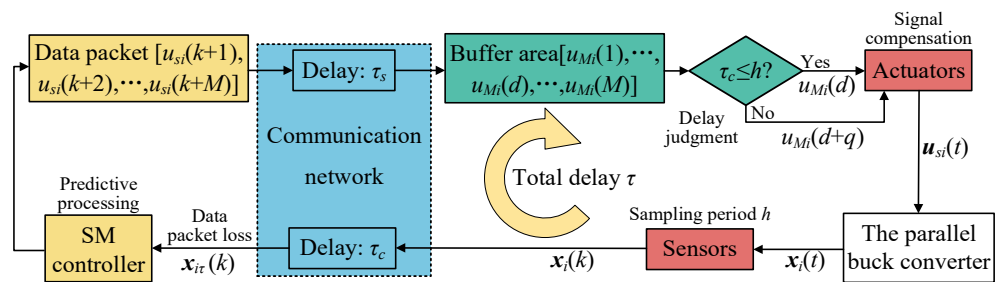


Figure 4. NCS signal transmission process based on multi-step prediction method.

As shown in Figure 4, since the upper bound of the NCS signal transmission delay is Mh , a buffer $u_{Mi} = [u_{Mi}(1), u_{Mi}(2), \dots, u_{Mi}(d), \dots, u_{Mi}(M)]$ of length M can be added in front of the actuator to store the pre-predicted control quantity u_{si} , and the initial value of all elements in u_{Mi} is zero. By sampling the system output signal every single sampling period h , the obtained sampled data $x_{i\tau}(k)$ is sent to the LSM controller by the transmission delay τ_c ; the designed LSM controller generates control signal packet $u_{si}(k + p)$ ($p = 1, 2, \dots, M$) according to the current system state $x_{i\tau}(k)$ prediction; after the $u_{si}(k + p)$ enters the buffer after the transmission delay τ_s , and is loaded into the corresponding u_{Mi} in order to be stored, and then the required $u_{Mi}(d)$ is transmitted to the actuator after the delayed judgment, so as to complete the effective compensation of the system transmission delay within the current h sampling period. It is worth noting that when the packet or actual sample data $x_i(k) = [x_{1i}(t), x_{2i}(t)]^T$ with $v_{O\tau}$, cannot be updated in real-time due to the delay τ_c greater than h , the buffer will transmit the control signal $u_{Mi}(d + q)$ to the actuator in order, where q represents the integer quotient of τ_c divided by h , so as to achieve uninterrupted sequential compensation control.

Remark 3. It should be noted here that in the multi-step prediction-based the NCS shown in Figure 4, both τ_c and τ_s are taken into account in the feedback system. The relationship between τ_c and h directly influences the state of the control signal compensated to the system actuator, while the size of τ_c and τ_s jointly affects the determination of the upper limit of the transmission delay M . This paper determines whether τ_c is greater than h by evaluating the equality of system states $x_{i\tau}(k)$ and $x_{i\tau}(k + 1)$, which cleverly takes the advantage of the fact that when $\tau_c > h$, sensors will transmit

the system state saved at the last time when the next sampling time h arrives, avoiding the trouble caused by the delay monitoring of the NCS.

Based on the analysis mentioned above, the crucial step for the compensation system to uphold its efficient output lies in acquiring the buffer control amount u_{Mi} . Hence, the subsequent paragraphs will outline the entire design procedure for the sliding mode controller based on the prediction method, which is shown in Figure 5.

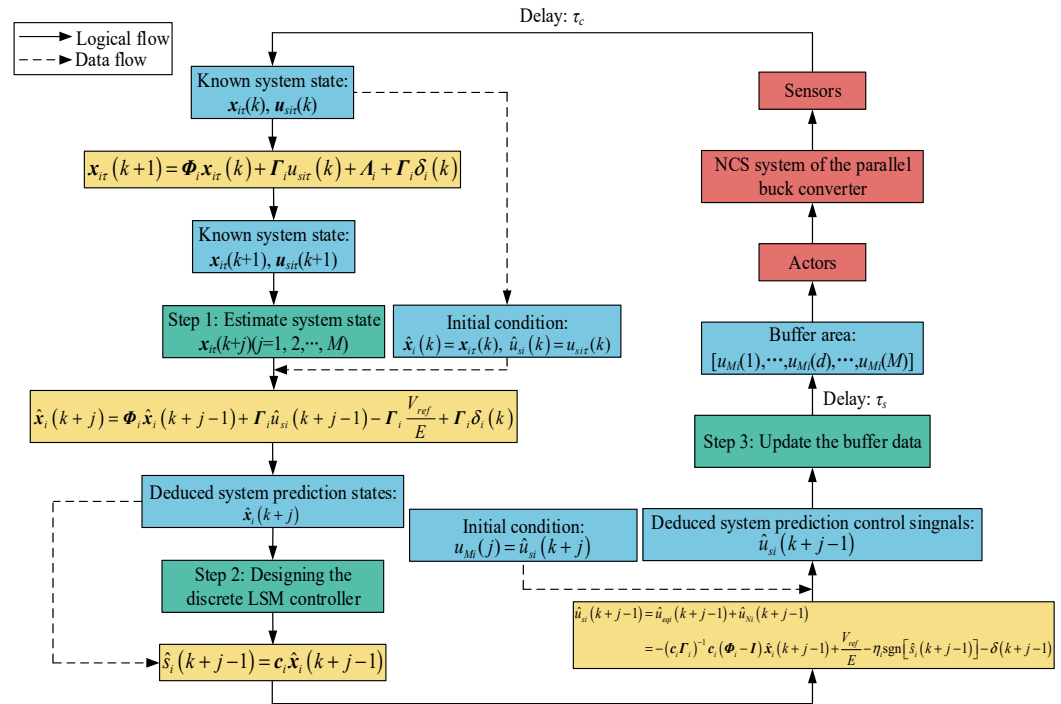


Figure 5. Design flow chart of the LSM controller based on multi-step prediction method.

Step 1: Estimate system state $x_{i\tau}(k+j)$ ($j = 1, 2, \dots, M$) based on sampled data $x_{i\tau}(k)$.

In the discrete model of (13), when $x_{i\tau}(k)$ and $u_{si\tau}(k)$ are known, $x_i(k+1)$ and $u_{si\tau}(k+1)$ can be obtained. In this way, the system state prediction formula can be designed as

$$\hat{x}_i(k+j) = \Phi_i \hat{x}_i(k+j-1) + \Gamma_i \hat{u}_{si}(k+j-1) - \Gamma_i \frac{V_{ref}}{E} + \Gamma_i \delta_i(k) \quad (24)$$

where $\hat{x}_i(k+j)$ is the estimated value of system state $x_{i\tau}(k+j)$ after the j -th sampling period predicted by state $x_{i\tau}(k)$; and there is $\hat{x}_i(k) = x_{i\tau}(k)$; $\hat{u}_{si}(k+j-1)$ is the control signal corresponding to the predicted state and satisfying $\hat{u}_{si}(k) = u_{si\tau}(k)$. Since the M times sampling period needs to be estimated backwards, the number of elements \hat{u}_{si} is M , and the initial value of each element is zero. For $\hat{x}_i(k) = x_{i\tau}(k)$ and $\hat{u}_{si}(k) = u_{si\tau}(k)$, this will be further explained later in terms of estimated errors. In the process of algorithm implementation, by using the iterative relationship shown in (24), the predicted state $\hat{x}_i(k+j)$ of the system at the next time can be obtained to acquire the system-predicted control signal $\hat{u}_{si}(k+j-1)$.

Step 2: Discrete the LSM controller is designed based on the predicted state.

As seen from (24), in order to obtain $\hat{x}_i(k+j)$, the control signal $\hat{u}_{si}(k+j-1)$ must be obtained first. The discrete LSM surface corresponding to a can be obtained from (14) that:

$$\hat{s}_i(k+j-1) = c_i \hat{x}_i(k+j-1) \quad (25)$$

By substituting (15) and (16) into (25), the equivalent control law $\hat{u}_{eqi}(k+j)$ and $\hat{u}_{Ni}(k+j)$ the switching control law can be obtained respectively as:

$$\hat{u}_{eqi}(k+j-1) = -(c_i \Gamma_i)^{-1} c_i (\Phi_i - I) \hat{x}_i(k+j-1) + \frac{V_{ref}}{E} - \delta(k+j-1) \quad (26)$$

$$\hat{u}_{Ni}(k+j-1) = -\eta_i \text{sgn}[\hat{s}_i(k+j-1)] \quad (27)$$

The control law $\hat{u}_{si}(k+j-1)$ can be further obtained by combining (25) and (26) as:

$$\begin{aligned} \hat{u}_{si}(k+j-1) &= \hat{u}_{eqi}(k+j-1) + \hat{u}_{Ni}(k+j-1) \\ &= -(c_i \Gamma_i)^{-1} c_i (\Phi_i - I) \hat{x}_i(k+j-1) + \frac{V_{ref}}{E} - \eta_i \text{sgn}[\hat{s}_i(k+j-1)] - \delta(k+j-1) \end{aligned} \quad (28)$$

Therefore, after $x_{i\tau}(k)$ is obtained from each sampling period, $\hat{u}_{si}(k+j-1)$ and $\hat{x}_{i\tau}(k+j)$ in the following M sampling periods can be predicted by steps 1 and 2 respectively, $\hat{u}_{si}(k+j-1)$ can also be turned into a switching signal $\hat{u}_i(k+j-1)$ by PWM as shown in (10). Hence, the predicted control signals in the controller buffer are continuously supplemented.

Step 3: Update the buffer data with predictive control signals.

The M predictive control signals obtained in step 2 are arranged in sequence and sent to the buffer in a unified package to update the data in u_{Mi} , that is, $u_{Mi}(j) = \hat{u}_{si}(k+j)$. After that, the system will select the corresponding $u_{Mi}(d)$ according to the measured system transmission delay τ and send it to the actuator. If the data in the buffer is not updated and the next sampling period has been entered at this time, the system will successively send $u_{Mi}(d+1)$ and subsequent control signals in the buffer to the actuator to ensure the continuity of the output signals of the controller, and the converter maintains stable operation; if the buffer has been updated, repeat step 3.

By repeating the above steps according to the sampling time h , the transmission delay of the NCS signal in the parallel buck converter can be compensated.

4.2. System Stability Analysis

The approach proposed in this paper aims to use the current system state for predicting future state quantities, enabling the proactive acquisition of corresponding control quantities to compensate for signal transmission delays. Thus, the crucial aspect of analyzing system stability lies in evaluating the accuracy of these predictions. This paper introduces an error variable following, which indicates the discrepancy between the estimated value and the actual value of the subsequent system:

$$e_i(j) = x_{i\tau}(k+j) - \hat{x}_i(k+j) \quad (29)$$

where $e_i(j)$ represents the deviation between the actual state value of the system and the true state value. And the expression of $x_{i\tau}(k+j)$ can be obtained from (13) as:

$$x_{i\tau}(k+j) = \Phi_i x_{i\tau}(k+j-1) + \Gamma_i u_{si\tau}(k+j-1) - \Gamma_i \frac{V_{ref}}{E} + \Gamma_i \delta_i(k+j-1) \quad (30)$$

Further substitute (24) and (30) into Equation (29) to obtain:

$$\begin{aligned} e_i(j) &= \Phi_i^j x_{i\tau}(k) + \Phi_i^{(j-1)} \Gamma_i u_{si}(k) + \dots + \Phi_i \Gamma_i u_{si}(k+j-2) + \Gamma_i u_{si}(k+j-1) + \Phi_i^{(j-1)} \Gamma_i \delta_i(k) + \dots + \Phi_i \Gamma_i \delta_i(k+j-2) \\ &+ \Gamma_i \delta_i(k+j-1) - \Phi_i^j x_{i\tau}(k) - \Phi_i^{(j-1)} \Gamma_i u_{si}(k) - \dots - \Phi_i \Gamma_i \hat{u}_{si}(k+j-2) - \Gamma_i \hat{u}_{si}(k+j-1) \\ &= \sum_{q=0}^{j-1} \Phi_i^q \Gamma_i \delta_i(k+j-1-q) \end{aligned} \quad (31)$$

According to the design idea of the buffer, its memory length should meet $M \geq d$. Since d is constant, the control signal predicted by the sampled system state $x_{iT}(k)$ is $\hat{u}_{si}(k+d)$, which corresponds to the LSM surface $\hat{s}_i(k+d)$. The Lyapunov equation can also be designed as:

$$\hat{V}_i(k+d) = \hat{s}_i^2(k+d) \tag{32}$$

According to the stability conditions of the discrete LSMC system, in order to ensure the stability of the multi-step predictive control system, (32) must meet the following conditions:

$$\Delta \hat{V}_i(k+d) = \hat{V}_i(k+d+1) - \hat{V}_i(k+d) = \hat{s}_i^2(k+d+1) - \hat{s}_i^2(k+d) < 0 \tag{33}$$

For ease of analysis, Equation (32) can be further rewritten as:

$$\Delta \hat{V}_i(k+d) = [\hat{s}_i(k+d+1) - \hat{s}_i(k+d)]^2 + 2\hat{s}_i(k+d)[\hat{s}_i(k+d+1) - \hat{s}_i(k+d)] < 0 \tag{34}$$

Let $\Delta \hat{s}_i(k+d) = \hat{s}_i(k+d+1) - \hat{s}_i(k+d)$, then from (24) to (29) we can get:

$$\begin{aligned} \Delta \hat{s}_i(k+d) &= \hat{s}_i(k+d+1) - \hat{s}_i(k+d) = \mathbf{c}_i \hat{\mathbf{x}}_i(k+d+1) - \mathbf{c}_i \hat{\mathbf{x}}_i(k+d) \\ &= \mathbf{c}_i \Phi_i \mathbf{e}_i(d) - \mathbf{c}_i \mathbf{e}_i(d+1) + \mathbf{c}_i \Gamma_i \hat{u}_{Ni}(k+d) + \mathbf{c}_i \Gamma_i \delta_i(k+d) \end{aligned} \tag{35}$$

By substituting (35) into (34), there is:

$$\begin{aligned} \Delta \hat{V}_i(k+d) &= \Delta \hat{s}_i(k+d)^2 + 2\hat{s}_i(k+d)\Delta \hat{s}_i(k+d) \\ &= [\mathbf{c}_i \Phi_i \mathbf{e}_i(d) - \mathbf{c}_i \mathbf{e}_i(d+1) + \mathbf{c}_i \Gamma_i \hat{u}_{Ni}(k+d) + \mathbf{c}_i \Gamma_i \delta_i(k+d)]^2 \\ &\quad + 2\hat{s}_i(k+d)[\mathbf{c}_i \Phi_i \mathbf{e}_i(d) - \mathbf{c}_i \mathbf{e}_i(d+1) + \mathbf{c}_i \Gamma_i \hat{u}_{Ni}(k+d) + \mathbf{c}_i \Gamma_i \delta_i(k+d)] < 0 \end{aligned} \tag{36}$$

In (36), without considering $\hat{s}_i(k+d) = 0$, it can be divided into $\hat{s}_i(k+d) > 0$ and $\hat{s}_i(k+d) < 0$ to discuss system stability:

(1) When $\hat{s}_i(k+d) > 0$, from (36) we can get:

$$\begin{aligned} \Delta \hat{V}_i(k+d) &= \Delta \hat{s}_i(k+d)^2 + 2\hat{s}_i(k+d)\Delta \hat{s}_i(k+d) \\ &= [\mathbf{c}_i \Phi_i \mathbf{e}_i(d) - \mathbf{c}_i \mathbf{e}_i(d+1) + \mathbf{c}_i \Gamma_i \hat{u}_{Ni}(k+d) + \mathbf{c}_i \Gamma_i \delta_i(k+d)]^2 \\ &\quad + 2\hat{s}_i(k+d)[\mathbf{c}_i \Phi_i \mathbf{e}_i(d) - \mathbf{c}_i \mathbf{e}_i(d+1) + \mathbf{c}_i \Gamma_i \hat{u}_{Ni}(k+d) + \mathbf{c}_i \Gamma_i \delta_i(k+d)] \\ &\leq \left[\sum_{q=0}^{d-1} |\mathbf{c}_i \Phi_i^{(q+1)} \Gamma_i \beta_i| - \sum_{p=0}^d |\mathbf{c}_i \Phi_i^p \Gamma_i \beta_i| + |\mathbf{c}_i \Gamma_i \beta_i| + \mathbf{c}_i \Gamma_i \hat{u}_{Ni}(k+d) \right]^2 \\ &\quad + 2\hat{s}_i(k+d) \left[\sum_{q=0}^{d-1} |\mathbf{c}_i \Phi_i^{(q+1)} \Gamma_i \beta_i| - \sum_{p=0}^d |\mathbf{c}_i \Phi_i^p \Gamma_i \beta_i| + |\mathbf{c}_i \Gamma_i \beta_i| + \mathbf{c}_i \Gamma_i \hat{u}_{Ni}(k+d) \right] \\ &= [\mathbf{c}_i \Gamma_i \hat{u}_{Ni}(k+d)]^2 + 2\hat{s}_i(k+d)\mathbf{c}_i \Gamma_i \hat{u}_{Ni}(k+d) < 0 \end{aligned} \tag{37}$$

Since $\hat{s}_i(k+d) > 0$, in order to ensure that the relationship in (36) holds, the parameters of the control system need to meet the following conditions:

$$\begin{cases} \mathbf{c}_i \Gamma_i \hat{u}_{Ni}(k+d) < 0 \\ 2\hat{s}_i(k+d) > -\mathbf{c}_i \Gamma_i \hat{u}_{Ni}(k+d) \end{cases} \tag{38}$$

By substituting (27) into (38), (38) can be rewritten as:

$$\begin{cases} -\mathbf{c}_i \Gamma_i \eta_i < 0 \\ 2\hat{s}_i(k+d) > \mathbf{c}_i \Gamma_i \eta_i \end{cases} \tag{39}$$

When the sampling period h meets $0 < h < 2nRC_i$, $c_i\Gamma_i > 0$ is established by substituting c_i and Γ_i into (39). Since the switching gain $\eta_i > 0$, the establishment condition of (39) is

$$\hat{s}_i(k+d) > \frac{\left[\frac{Eh}{L_iC_i} + (\lambda_i + k_iS_{xi})\frac{Eh^2}{2L_iC_i} - \frac{Eh^2}{2nRL_iC_i^2} \right] \eta_i}{2} \tag{40}$$

(2) When $\hat{s}_i(k+d) < 0$, from (36) we can also get:

$$\Delta\hat{V}_i(k+d) = [c_i\Gamma_i u_{Ni}(k+d)]^2 + 2\hat{s}_i(k+d)c_i\Gamma_i\hat{u}_{Ni}(k+d) < 0 \tag{41}$$

Given that $\hat{s}_i(k+d) < 0$, it is essential to satisfy the following conditions for the parameters of the control system in order to maintain the validity of the relationship expressed in Equation (41):

$$\begin{cases} c_i\Gamma_i\hat{u}_{Ni}(k+d) > 0 \\ 2\hat{s}_i(k+d) < -c_i\Gamma_i\hat{u}_{Ni}(k+d) \end{cases} \tag{42}$$

And (42) can be rewritten as follows by further substituting (27) into it:

$$\begin{cases} c_i\Gamma_i\eta_i > 0 \\ 2\hat{s}_i(k+d) < -c_i\Gamma_i\eta_i \end{cases} \tag{43}$$

The parameter matrixes c_i and Γ_i can also be substituted into (43) as:

$$\hat{s}_i(k+d) < -\frac{\left[\frac{Eh}{L_iC_i} + (\lambda_i + k_iS_{xi})\frac{Eh^2}{2L_iC_i} - \frac{Eh^2}{2nRL_iC_i^2} \right] \eta_i}{2} \tag{44}$$

According to (40) and (44), the stability condition of the multi-step predictive control system designed in this paper can be expressed as:

$$0 < \frac{c_i\Gamma_i\eta_i}{2} < |\hat{s}_i(k+d)| \tag{45}$$

From (45), the results show that the system state will eventually converge to the vicinity of the SM surface as:

$$s_i^A = \left\{ s_i(k+j) \left| -\frac{c_i\Gamma_i\eta_i}{2} \leq \hat{s}_i(k+d) \leq \frac{c_i\Gamma_i\eta_i}{2} \right. \right\} \tag{46}$$

5. Simulation and Experimental Verification

5.1. Simulation Analysis and Verification

The performance of the SMC system designed in this paper will be evaluated through simulations. Specifically, the output current and system control quantity for phase i of the parallel buck converter's NCS will be investigated. The sampling period is set to $h = 0.1$ ms, and the controller parameters are set as $\lambda_i = 600$, $k_i = 100$. Random delays τ , ranging from $[0, 0.2$ ms], $[0, 0.4$ ms], and $[0, 0.6$ ms], will be introduced to the NCS, and τ_s and τ_c obtain the delay randomly assigned by τ , while keeping the parameters in Table 1 unchanged. And the random noise disturbance of 0–1 V is superimposed on the input of each phase of the control signal of the buck converter. Table 3 and Figure 6 below show the simulation results before and after processing with the delay signal compensation.

Table 3. System performance results before and after delay compensation in different intervals.

τ (ms)	Compensated State	$\Delta v_{O\tau}$ (V)	$\Delta v_{O\tau_max}$ (V)	$\Delta i_{Li\tau}$ (A)	$\Delta i_{Li\tau_max}$ (A)	System Current Mode
0.2	No	0.22	0.78	1.02	0.44	CCM
	Yes	0.02	0.01	0.81	0.37	CCM
0.4	No	0.31	2.96	1.29	1.01	DCM
	Yes	0.08	1.58	1.03	0.45	CCM
0.6	No	0.35	2.41	1.61	1.39	DCM
	Yes	0.11	1.42	1.38	0.67	CCM

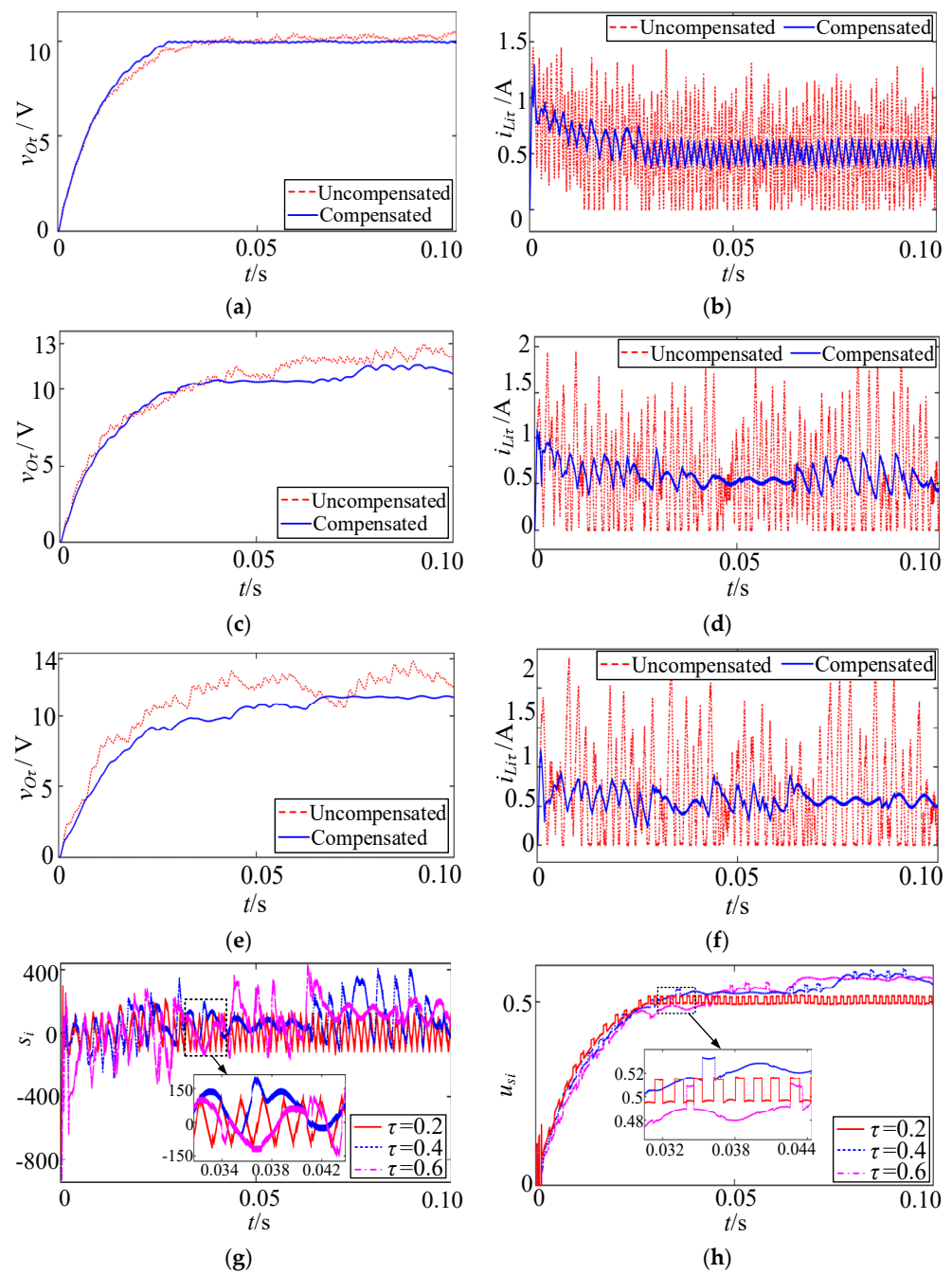


Figure 6. The output performance of NCS before and after compensation under different delays: (a) $v_{O\tau}$ in 0.2 ms delay; (b) $i_{Li\tau}$ in 0.2 ms delay; (c) $v_{O\tau}$ in 0.4 ms delay; (d) $i_{Li\tau}$ in 0.4 ms delay; (e) $v_{O\tau}$ in 0.6 ms delay; (f) $i_{Li\tau}$ in 0.6 ms delay; (g) s_i in long delays; (h) u_{si} in long delays.

The system output $v_{O\tau}$, before and after compensation, under different intervals of long delay are presented in Figure 6a,c,e. When the delay τ falls in $[0, 0.2 \text{ ms}]$, it can be seen that the compensated $v_{O\tau}$ is 0.2 V lower than the uncompensated voltage fluctuation, and the dynamic response time of the voltage is nearly 0.01 s higher, and the maximum voltage error $\Delta v_{O\tau_max}$ is reduced from 0.78 V to 0.01 V by compensation. When the delay τ further increases to the range with $[0, 0.4 \text{ ms}]$, the uncompensated $v_{O\tau}$ shows more violent fluctuations, and the steady-state error reached 0.31 V, while the compensated $v_{O\tau}$ remained stable, with only 0.08 V steady-state error, and the $\Delta v_{O\tau_max}$ is also reduced 1.38 V. When the τ falls in the range $[0, 0.2 \text{ ms}]$, it can be seen from the uncompensated $v_{O\tau}$ that the transmission of the control signal of the system is seriously damaged at this time, and the $\Delta v_{O\tau}$ and $\Delta v_{O\tau_max}$ reach 0.35 V and 2.41 V, respectively. However, they can be reduced by 0.24 V and 0.99 V through compensation, so that the voltage curve can remain stable, which also evidences that the addition of multi-step predictive control significantly reduces the fluctuation range of the output voltage and current, leading to a more stable system output.

Figure 6b,d,f show the system output current signal $i_{Li\tau}$ before and after compensation. With the increase in the system transmission signal delay τ , the fluctuation steady-state error $\Delta i_{Li\tau}$ of the uncompensated signal $i_{Li\tau}$ increases from 1.02 A to 1.61 A, and the maximum current error $\Delta i_{Li\tau_max}$ increases from 0.44 A to 1.39 A, almost doubling the rated current value, the $i_{Li\tau}$ also changes from CCM to DCM. While the fluctuating peak current will cause damage to the stability of the converter load. After the compensation controller is added, it can be seen that the $\Delta i_{Li\tau}$ decreases by 0.21 A, 0.26 A and 0.23 A, respectively, and the $\Delta i_{Li\tau_max}$ decreases by 0.07 A, 0.56 A, and 0.72 A, respectively, and the current stability increases significantly. It can further be observed that the enhanced NCS leads to the system output $i_{Li\tau}$ operating under CCM, which is attributed to the effective compensation of the multi-step predictive controller for losing the system control signal caused by delays.

Figure 6h visually confirms the continuity of the system control signal u_{si} . It can be observed that with the increase in system transmission delay τ , u_{si} gradually fluctuates, but it can remain continuous and stable under the compensation of the multiple unpredictable controller. When the τ reaches 4 times and 6 times the sampling time h , u_{si} can already remain near 0.5 in the initial 0.5 s to maintain the stable operation of the system. The improvement effectively mitigates the impact of long delays on system output performance, further enhancing the steady-state output performance of the parallel buck converter system.

Figure 6g demonstrates the sliding variable s_i of the system with different time delays after compensation. Thanks to the multi-step predictive controller, s_i maintains both continuity and stability despite delays. This not only leverages the characteristics of SMC but also ensures the system's strong robustness.

5.2. Experimental Verification

In this paper, the dSPACE1006 controller with powerful data computing capability is selected to verify the designed control strategy and some theories. The experimental platform of the parallel buck converter control system based on dSPACE1006 is established as shown in Figure 7a, and its operating process is illustrated in Figure 7b.

5.2.1. Verification of the Effect of Different Delays on NCS's Output Performance

Keep the converter circuit parameters consistent with those in Table 1. And the controller parameter $\lambda_i = 600$, $k_i = 100$ and the sampling period $h = 0.1 \text{ ms}$ are set unchanged, so that the signal transmission delay is within four random intervals of $[0, 0.1 \text{ ms}]$, $[0, 0.2 \text{ ms}]$, $[0, 0.4 \text{ ms}]$ and $[0, 0.6 \text{ ms}]$, respectively. The experimental results are shown in Table 4 and Figure 8 below.

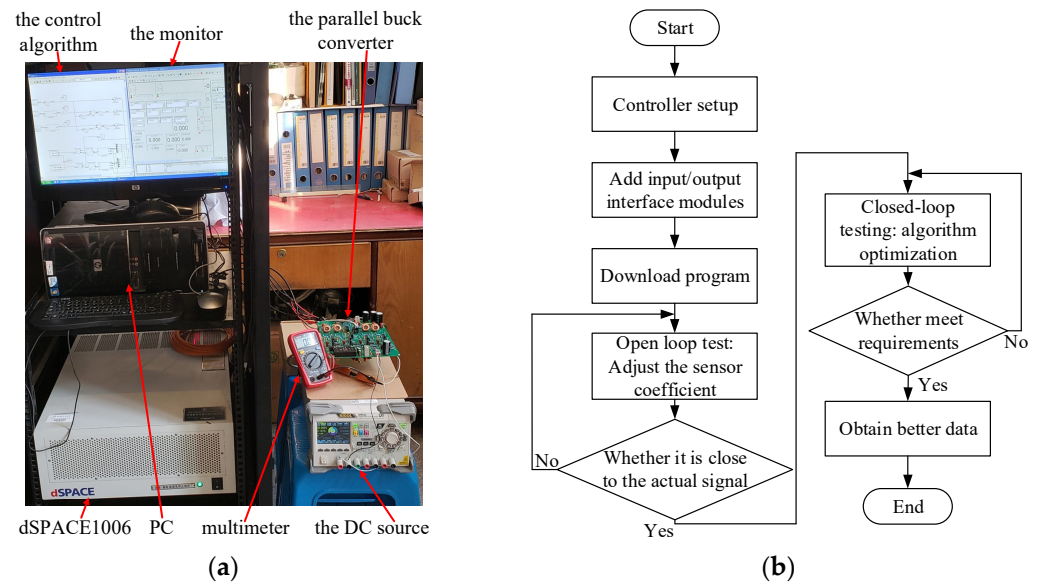


Figure 7. Illustration of the experimental platform based on the dSPACE1006: (a) experimental platform diagram; (b) experimental operation flow.

Table 4. System output voltage characteristics under different time delays.

τ (ms)	Rise Time (ms)	Mean Steady-State Error (V)	Maximum Amplitude Error (V)
0	103	0.22	0.37
0–0.1	122	0.40	0.50
0–0.2	138	0.74	1.01
0–0.4	148	0.89	1.41
0–0.6	173	0.91	1.61

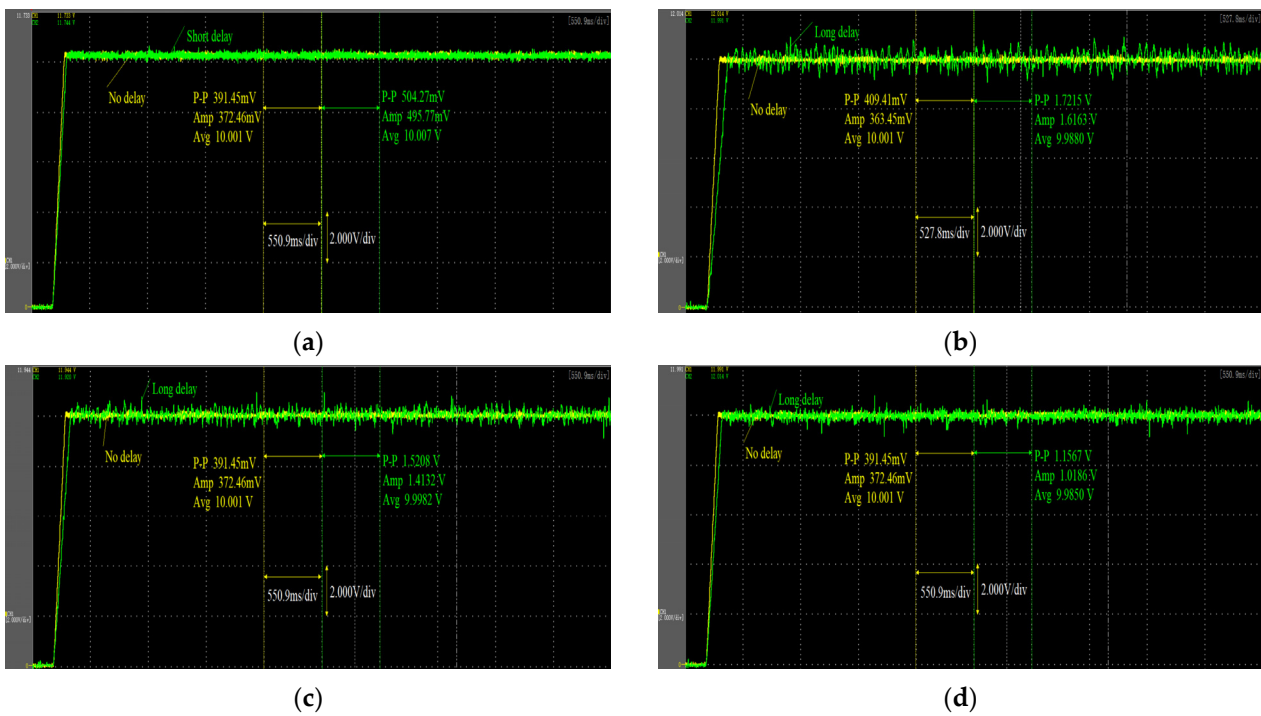


Figure 8. System output voltage $v_{O\tau}$ under different time delays: (a) $v_{O\tau}$ in 0.1 ms delay; (b) $v_{O\tau}$ in 0.2 ms delay; (c) $v_{O\tau}$ in 0.4 ms delay; (d) $v_{O\tau}$ in 0.6 ms delay.

The output voltage $v_{O\tau}$ shown in Figure 8a demonstrates that the presence of random delays in the NCS has minimal impact on the output voltage characteristics when the delay is equal to or less than one sampling period. Thus, the effect of this delay type on the system performance can be disregarded. However, further examination of Figure 8b–d and Table 4 reveals that as the transmission delay increases, both the rise time and the maximum error of the system output voltage increase. Precisely, when the random delay ranges from 0 to 0.2 ms, 0 to 0.4 ms, and 0 to 0.6 ms, the maximum error corresponds to values of 0.74 V, 0.89 V, and 0.91 V, respectively. These results indicate a poor steady-state performance that fails to meet the required performance standards, necessitating the implementation of delayed compensation processing. The experimental findings confirm that short delays have a negligible impact on the NCS performance, while longer delays adversely affect both the transient and steady-state performance of the control system and increase the steady-state error. These conclusions align with the outcome of the simulation analysis obtained in Figure 3.

5.2.2. Verification of Compensation Strategy for NCS Transmitted Delay Signal Based on Multi-Step Prediction Method

As seen from Figure 8 and Table 4, performing the control system with random delays of [0, 0.4 ms] and [0, 0.6 ms] is poor, hence, it is very important to compensate the long transmission delay of the NCS in the parallel buck converter, which is one of the important conclusions of this paper. The actual compensation effect of the LSM controller designed in this paper based on the multi-step prediction method to the long transmission delay of the system NCS will be verified by designed experiments.

Similarly, the 0–1 V random noise disturbance signal is superimposed on the input side of each phase control signal of the parallel buck converter. Here, typical random long transmission delay intervals [0, 0.4 ms] and [0, 0.6 ms] shown in Figure 8c,d are selected to verify the effectiveness of the designed controller, and the experimental results are shown in Table 5 and Figure 9.

Table 5. The output voltage characteristics before and after treatment with the multi-step prediction method.

τ (ms)	Compensated State	Rise Time (ms)	Mean Steady-State Error (V)	Maximum Amplitude Error (V)
0–0.4	No	148	0.89	0.99
	Yes	64	0.48	0.78
0–0.6	No	173	0.91	1.39
	Yes	67	0.57	0.62

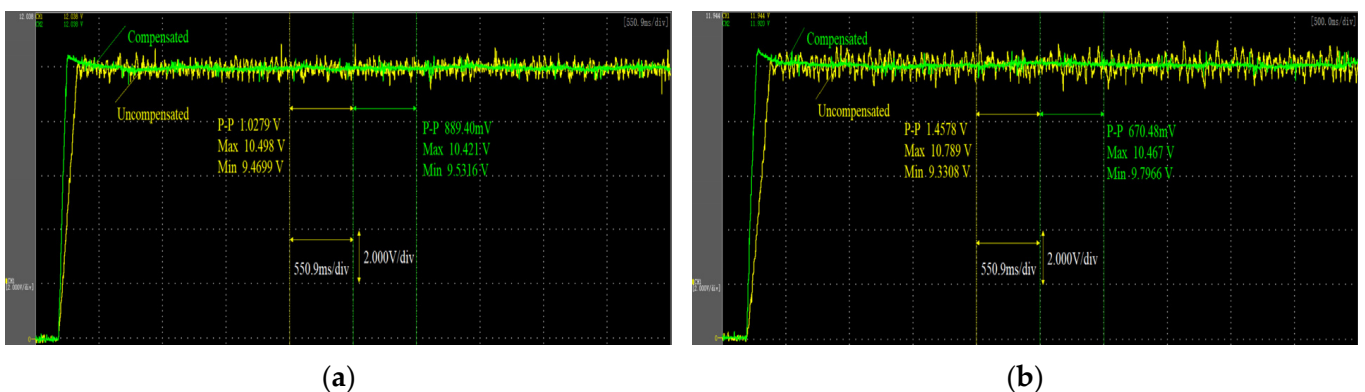


Figure 9. The experimental results of the system output voltage before and after the multistep prediction method: (a) $v_{O\tau}$ in 0.4 ms delay; (b) $v_{O\tau}$ in 0.6 ms delay.

As evidenced by the output voltage $v_{O\tau}$ presented in Figure 9 and the accompanying data in Table 5, both the buffer method and the multi-step prediction method effectively mitigate the adverse impact of signal transmission delay on the steady-state performance of NCS. This mitigation is reflected in a substantial reduction in the maximum error in the system's output voltage, from 0.89 V and 0.91 V to 0.48 V and 0.57 V, respectively, resulting in a marked improvement in steady-state performance. Following implementing delay compensation, the rise time of the system's output voltage decreases from 148 ms and 173 ms to 64 ms and 67 ms, respectively, signifying a noticeable enhancement in system response speed. It is worth noting that the system experiences an overshoot phenomenon, with overshoot values of 0.48 V and 0.57 V, respectively, because of employing advanced prediction techniques, which have a detrimental effect on transient performance. An examination of the output voltage waveform reveals sporadic occurrences of minor peaks during the steady-state phase. This observation underscores certain limitations in the multi's utilization-step prediction method for delay compensation.

6. Conclusions

In this paper, the effect of random long delay on the NCS performance of the parallel buck converter system is analyzed in detail. The results show that the effect of short delays on the system can be ignored, but long delays will increase the steady-state error of the system output and seriously affect the system's stability. Therefore, this paper proposes a sliding mode control strategy based on the multi-step prediction method. Firstly, the discrete domain model of the system and the LSM controller are constructed and constructed. On this basis, the influence of long delay and matching disturbance on the NCS is fully considered, and the compensation strategy of the multi-step prediction method is designed. Through the continuous supply of the predictive control quantity stored in the buffer, losing the NCS control signal in the case of long delays is compensated, thus easing the impact of signal transmission delay on the system performance and ensuring the stability of the system output. Finally, the multi-step predictive control strategy proposed in this paper demonstrates remarkable improvements in system performance through the designed experiments. On average, this strategy reduces the system's output steady-state error by 41.6%, while also reducing the output response time by 61.2% and the maximum error of the output signal by 20.6%. These significant improvements clearly validate the superiority of the proposed method, which proves the correction of the proposed method.

Author Contributions: Conceptualization, J.Y. and W.X.; methodology, W.Z.; software, W.Z.; validation, Y.W., J.Y. and W.X.; formal analysis, W.Z.; investigation, J.Y.; resources, W.X.; data curation, W.Z.; writing—original draft preparation, Y.W.; writing—review and editing, Y.W.; visualization, W.Z.; supervision, Y.W.; funding acquisition, Y.W. All authors have read and agreed to the published version of the manuscript.

Funding: This research was funded by the National Natural Science Foundation of China, grant number 51307035 and 62073095.

Data Availability Statement: Data are contained within the article.

Conflicts of Interest: Authors Juan Yu and Wenwen Xiong were employed by the company Yatai Construction Science & Technology Consulting Institute Co., Ltd. The remaining authors declare that the research was conducted in the absence of any commercial or financial relationships that could be construed as a potential conflict of interest.

References

1. Peng, D.; Huang, M.; Li, J.; Sun, J.; Zha, X.; Wang, C. Large-signal stability criterion for parallel-connected DC–DC converters with current source equivalence. *IEEE Trans. Circuits Syst. II Express Briefs* **2019**, *66*, 2037–2041. [[CrossRef](#)]
2. Li, H.; Ren, F.; Liu, C.; Guo, Z.; Lü, J.; Zhang, B.; Zheng, T.Q. An extended stability analysis method for paralleled dc-dc converters system with considering the periodic disturbance based on floquet theory. *IEEE Access* **2020**, *8*, 9023–9036. [[CrossRef](#)]
3. Shi, J.; Zhou, L.; Li, J.; He, X. Common-duty-ratio control of input-parallel output-parallel (IPOP) connected DC–DC converter modules with automatic sharing of currents. *IEEE Trans. Power Electron.* **2012**, *27*, 3277–3291. [[CrossRef](#)]

4. Panov, Y.; Jovanovic, M.M. Loop gain measurement of paralleled DC–DC converters with average-current-sharing control. *IEEE Trans. Power Electron.* **2008**, *23*, 2942–2948. [[CrossRef](#)]
5. Xu, G.; Sha, D.; Liao, X. Decentralized inverse-droop control for input-series–output-parallel DC–DC converters. *IEEE Trans. Power Electron.* **2015**, *30*, 4621–4625. [[CrossRef](#)]
6. Wang, R.; Liu, G.-P.; Wang, J.; Rees, D.; Zhao, Y.B. Guaranteed cost control for networked control systems based on an improved predictive control method. *IEEE Trans. Control Syst. Technol.* **2010**, *18*, 1226–1232. [[CrossRef](#)]
7. Klügel, M.; Mamduhi, M.; Ayan, O.; Vilgelm, M.; Johansson, K.H.; Hirche, S.; Kellerer, W. Joint cross-layer optimization in real-time networked control systems. *IEEE Trans. Control Netw. Syst.* **2020**, *7*, 1903–1915. [[CrossRef](#)]
8. Zhao, Y.-B.; Liu, G.-P.; Rees, D. Design of a packet-based control framework for networked control systems. *IEEE Trans. Control Syst. Technol.* **2009**, *17*, 859–865. [[CrossRef](#)]
9. Wu, C.; Liu, J.; Jing, X.; Li, H.; Wu, L. Adaptive fuzzy control for nonlinear networked control systems. *IEEE Trans. Syst. Man Cybern. Syst.* **2017**, *47*, 2420–2430. [[CrossRef](#)]
10. Xu, H.; Jagannathan, S. Neural network-based finite horizon stochastic optimal control design for nonlinear networked control systems. *IEEE Trans. Neural Netw. Learn. Syst.* **2015**, *26*, 472–485. [[CrossRef](#)]
11. Shi, Y.; Yu, B. Output feedback stabilization of networked control systems with random delays modeled by markov chains. *IEEE Trans. Autom. Control* **2009**, *54*, 1668–1674.
12. Qiu, J.; Gao, H.; Ding, S.X. Recent advances on fuzzy-model-based nonlinear networked control systems: A survey. *IEEE Trans. Ind. Electron.* **2016**, *63*, 1207–1217. [[CrossRef](#)]
13. Tavassoli, B. Stability of nonlinear networked control systems over multiple communication links with asynchronous sampling. *IEEE Trans. Autom. Control* **2014**, *59*, 511–515. [[CrossRef](#)]
14. Savkin, A.V.; Cheng, T.M. Detectability and output feedback stabilizability of nonlinear networked control systems. *IEEE Trans. Autom. Control* **2007**, *52*, 730–735. [[CrossRef](#)]
15. Liu, K.-Z.; Wang, R.; Liu, G.-P. Tradeoffs between transmission intervals and delays for decentralized networked control systems based on a gain assignment approach. *IEEE Trans. Circuits Syst. II Express Briefs* **2016**, *63*, 498–502. [[CrossRef](#)]
16. Maity, D.; Mamduhi, M.H.; Hirche, S.; Johansson, K.H. Optimal lqg control of networked systems under traffic-correlated delay and dropout. *IEEE Control Syst. Lett.* **2022**, *6*, 1280–1285. [[CrossRef](#)]
17. Tang, B.; Wang, J.; Zhang, Y. A delay-distribution approach to stabilization of networked control systems. *IEEE Trans. Control Netw. Syst.* **2015**, *2*, 382–392. [[CrossRef](#)]
18. Tan, C.; Zhang, H. Necessary and sufficient stabilizing conditions for networked control systems with simultaneous transmission delay and packet dropout. *IEEE Trans. Autom. Control* **2017**, *62*, 4011–4016. [[CrossRef](#)]
19. Shangguan, X.-C.; Zhang, C.-K.; He, Y.; Jin, L.; Jiang, L.; Spencer, J.W.; Wu, M. Robust load frequency control for power system considering transmission delay and sampling period. *IEEE Trans. Ind. Inform.* **2021**, *17*, 5292–5303. [[CrossRef](#)]
20. Pang, H.-p.; Liu, C.-j.; Liu, A.-z. Sliding Mode Control for Time-DELAY systems with Its Application to Networked Control Systems. In Proceedings of the Sixth International Conference on Intelligent Systems Design and Applications, Jian, China, 16–18 October 2006; pp. 192–197.
21. Yan, S.; Shen, M.Q.; Nguang, S.K.; Zhang, G.M. Event-triggered H_∞ control of networked control systems with distributed transmission delay. *IEEE Trans. Autom. Control* **2020**, *65*, 4295–4301. [[CrossRef](#)]
22. Kim, D.S.; Choi, D.H.; Mohapatra, P. Real-time scheduling method for networked discrete control systems. *Control Eng. Pract.* **2009**, *17*, 564–570. [[CrossRef](#)]
23. Heemels, W.P.M.H.; Teel, A.R.; van de Wouw, N.; Nesic, D. Networked control systems with communication constraints: Tradeoffs between transmission intervals, delays and performance. *IEEE Trans. Autom. Control* **2010**, *55*, 1781–1796. [[CrossRef](#)]
24. Padhy, B.P.; Srivastava, S.C.; Verma, N.K. A Wide-Area Damping Controller Considering Network Input and Output Delays and Packet Drop. *IEEE Trans. Power Syst.* **2017**, *32*, 166–176. [[CrossRef](#)]
25. Liu, G.P.; Chai, S.C.; Mu, J.X.; Rees, D. Networked Predictive Control of Systems with Random Delay in Signal Transmission Channels. *Int. J. Syst. Sci.* **2008**, *39*, 1055–1064. [[CrossRef](#)]
26. Huangfu, Y.; Ma, R.; Zhao, B.; Liang, Z.; Ma, Y.; Wang, A.; Zhao, D.; Li, H.; Ma, R. A novel robust smooth control of input parallel output series quasi-z-source DC–DC converter for fuel cell electrical vehicle applications. *IEEE Trans. Ind. Appl.* **2021**, *57*, 4207–4221. [[CrossRef](#)]
27. Mosayebi, M.; Gheisarnejad, M.; Khooban, M.H. An intelligent sliding mode control for stabilization of parallel converters feeding cpls in DC-microgrid. *IET Power Electron.* **2022**, *15*, 1596–1606. [[CrossRef](#)]
28. Lee, S.; Jeung, Y.-C.; Lee, D.-C. Voltage balancing control of ipos modular dual active bridge DC/DC converters based on hierarchical sliding mode control. *IEEE Access* **2019**, *7*, 9989–9997. [[CrossRef](#)]
29. Wei, Z.; Zhang, W.; Wang, Y. Sliding mode control for parallel DC–DC converter network systems with uniform quantization and discretization effects. *IEEE Access* **2023**, *11*, 99918–99934. [[CrossRef](#)]
30. Lopez, M.; Vicuna, L.G.; Castilla, M.; Gaya, P.; Lopez, O. Current distribution control design for paralleled DC/DC converters using sliding-mode control. *IEEE Trans. Ind. Electron.* **2004**, *51*, 419–428. [[CrossRef](#)]
31. Taheri, B.; Sedaghat, M.; Bagherpour, M.A.; Farhadi, P. A New Controller for DC-DC Converters Based on Sliding Mode Control Techniques. *J. Control. Autom. Electr. Syst.* **2019**, *30*, 63–74. [[CrossRef](#)]

32. Alsmadi, Y.; Utkin, V.; Haj-ahmed, M.; Xu, L. Sliding mode control of power converters: DC/DC converters. *Int. J. Control* **2018**, *91*, 2472–2493. [[CrossRef](#)]
33. Zhao, Y.; Qiao, W.; Ha, D. A sliding-mode duty-ratio controller for DC/DC buck converters with constant power loads. *IEEE Trans. Ind. Appl.* **2014**, *50*, 1448–1458. [[CrossRef](#)]

Disclaimer/Publisher’s Note: The statements, opinions and data contained in all publications are solely those of the individual author(s) and contributor(s) and not of MDPI and/or the editor(s). MDPI and/or the editor(s) disclaim responsibility for any injury to people or property resulting from any ideas, methods, instructions or products referred to in the content.